14th International Symposium on Turbulence and Shear Flow Phenomena (TSFP14)
Heidelberg, Germany, July 28-31, 2026

CONTRIBUTION OF LARGE-SCALE STRUCTURES TO WALL SHEAR STRESS IN DRAG-REDUCED POLYMER TURBULENCE

Jumpei Asaoka
Department of Energy Engineering and Science, Graduate School of Engineering, Nagoya University, Furo-Cho, Chikusa-Ku, Nagoya City, Aichi Prefecture 464-8603, Japan
asaoka.jumpei.m4@s.mail.nagoya-u.ac.jp

Yuta Yamamoto
Department of Energy Engineering and Science, Graduate School of Engineering, Nagoya University, Furo-Cho, Chikusa-Ku, Nagoya City, Aichi Prefecture 464-8603, Japan
yuta.yamamoto1114@gmail.com

Yu Wang
Department of Energy Engineering and Science, Graduate School of Engineering, Nagoya University, Furo-Cho, Chikusa-Ku, Nagoya City, Aichi Prefecture 464-8603, Japan
wang.yu.k1@foxmail.com

Yoshiyuki Tsuji
Department of Energy Engineering and Science, Graduate School of Engineering, Nagoya University, Furo-Cho, Chikusa-Ku, Nagoya City, Aichi Prefecture 464-8603, Japan
c42406a@nucc.cc.nagoya-u.ac.jp

ABSTRACT

This study aimed to elucidate the drag reduction mechanism in turbulent polymer-added flow by examining the relationship between the velocity field and wall shear stress. Channel flow experiments were conducted with polyacrylamide concentrations from 0 to 300 ppm. The two-dimensional velocity field (streamwise–wall-normal) was measured using PIV, while wall shear stress was simultaneously obtained by an electrochemical method, which, through a modified electrode arrangement, allowed measurements in both streamwise and spanwise directions. At a friction Reynolds number of $Re_\tau = 440$, a maximum drag reduction of 21% was achieved at 300 ppm. To investigate the mechanism, correlation analysis was performed between wall shear stress and the velocity field, focusing on large-scale motions known as LSM/VLSM, by extracting their long-wavelength components. Recent studies have suggested that large-scale structures near the free stream influence the turbulence in the near-wall region, and this study investigated that influence (Marusic and Hutchins, 2007). The present results showed that increasing polymer concentration progressively confined the strong correlation between large-scale motions and wall shear stress to the near wall region and ultimately weakened it sharply. These findings indicate that polymers effectively block the influence of large-scale motions on the wall, thereby contributing to drag reduction.

INTRODUCTION

Enhancing the transport efficiency of fluid systems requires reducing frictional losses in turbulent flows. A landmark discovery by Toms in 1948 showed that adding minute amounts of polymer to a fluid can dramatically reduce turbulent frictional drag (Toms, 1949). This phenomenon, known as the Toms effect, enables drag reduction of up to 80% at polymer concentrations of only a few tens of parts per million.

Previous studies have suggested that polymer-induced drag reduction is closely related to modifications of coherent structures in the near-wall region of turbulence. Kline et al. first identified elongated low-speed streaks near the edge of the viscous sublayer (Kline et al., 1967), and subsequent experimental investigations reported that polymer additives attenuate turbulence intensity, particularly by suppressing wall-normal velocity fluctuations (Li, 2019; Kim et al., 2004; Kim et al., 2005).

Recent advances in particle image velocimetry (PIV) and numerical simulations have highlighted the importance of large-scale motions (LSMs) and very-large-scale motions (VLSMs) in turbulent transport and wall friction (Mathis, 2009). While these structures are known to influence momentum transfer across the channel, their interaction with polymer dynamics and the resulting effect on wall shear stress remain unclear.

In the present study, simultaneous measurements of velocity fields using PIV and wall shear stress using an electrochemical technique are conducted in polymer drag-reducing flows. The objective is to clarify how large-scale turbulent structures influence wall shear stress and to provide further insight into the mechanisms of polymer-induced drag reduction.

EXPERIMENTAL CONDITIONS

This section outlines the experimental conditions and the measurement principles of the techniques used in this study. Two measurement methods were applied: Particle Image Velocimetry (PIV) for capturing the velocity field and an electrochemical technique for determining the wall shear stress. Both measurements were conducted at the same location in the flow. In the electrochemical system, rectangular electrodes were arranged in a V-shaped configuration, allowing the wall shear stress components to be evaluated in both the streamwise and spanwise directions.

The wall shear stress is defined by $\tilde{\tau}_{w,i} = \tau_{w,i} + \tau_{w,i}{}'$, where $i = x, z$, $\tilde{\tau}_w$ is the instantaneous wall shear stress, τ_w is the mean wall shear stress, and $\tau_w{}'$ is the fluctuating component. Vector $\tilde{\boldsymbol{\tau}}_{\boldsymbol{w}}$ is defined as $\tilde{\boldsymbol{\tau}}_{\boldsymbol{w}} = (\tilde{\tau}_{w,x}, \tilde{\tau}_{w,z})$. Similarly, the mass transfer coefficient is defined by $\tilde{k}_i = k_i + k_i{}'$, where $i = x, z$, $\tilde{k}$ represents the instantaneous mass transfer rate, and k and k' are its mean and fluctuation, respectively. The streamwise velocity is defined by $\tilde{u} = U + u'$, where $\tilde{u}$ is the instantaneous velocity, U and u' are its mean and fluctuating component.

Experimental setup

The flow loop consisted of an acrylic channel duct as the test section, followed by a circular tube, a tank, a pump, and a flow meter. The channel duct's test section has a hole for the working electrode plate and a Ni plate for the counter electrode. The channel duct measures 10 mm in height, 120 mm in width, and 2040 mm in length. The distance from the channel inlet to the test section is 1330 mm, ensuring the flow is fully developed before reaching the measurement point.

A tank was prepared to hold a sufficient amount of solution for the test loop and to inject nitrogen gas to reduce the concentration of dissolved oxygen. The tank was equipped with a nitrogen gas supply line, and a hole was made in the lid to insert a dissolved oxygen meter. An Iwaki Co., Ltd. centrifugal pump (model X-402RV6-2) was used to drive the liquid through the channel. The internal impeller of this pump is resin-coated, which prevents metal-fluid contact, making it suitable for electrochemical experiments that require the use of an electrolyte. A FLOW-CELL Co., Ltd. electromagnetic flow meter (model MCY-111A) with an accuracy of ±0.5% was used to measure the flow rate within the channel. The total amount of electrolyte used during the experiment was approximately 70 L, while the tank had a capacity of 200 L. A 20 L plastic tank was placed inside the main tank to slightly raise the water level. The circuit's outlet inside the tank was positioned underwater as far as possible from the pump's inlet. The working electrode was located downstream of the counter and reference electrodes. To minimize the interference of electrical noise, the cables were wrapped in aluminum foil and grounded during the experiment (Wang and Tsuji, 2024).

PIV (Particle Image Velocimetry)

To observe the two-dimensional velocity field in the streamwise and wall-normal directions, a laser sheet was introduced from above to illuminate the central region of the channel, while a high-speed camera was positioned laterally to capture particle images. A schematic illustration of the PIV measurement setup is presented in Figure 1. Illumination was provided by a continuous-wave (CW) laser with a wavelength of 532 nm. Nylon tracer particles with a mean diameter of 4.1 µm and a density of 1.02 g/cc were seeded into the flow.

The recorded particle images were processed using the commercial PIV software DAVIS 10.1 to obtain the instantaneous velocity fields. The measurement window covered a square area of 5 mm × 5 mm, extending from the channel bottom wall to the channel half-height. Image acquisition was performed with a spatial resolution of 512 × 512 pixels (corresponding to 9.7 × 9.7 µm per pixel) at a sampling rate of 4 kHz. The electrochemical wall shear stress measurements were conducted at the same sampling frequency to ensure temporal synchronization with the PIV data.

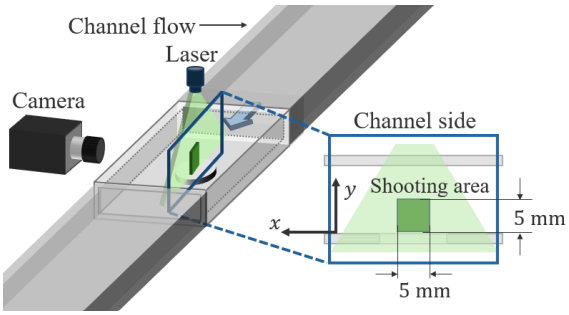

Figure 1. Experimental setups for PIV imaging system

The electrochemical method

Determining the mass transfer coefficient. The electrochemical measurement method was adopted to directly calculate the mass transfer coefficient by continuously measuring time-series data [9]. This technique determines the mass transfer coefficient by measuring the current generated by the oxidation-reduction reaction of ions (chemical species) in an electrolyte solution at an electrode surface. When a voltage is applied to the electrodes, a reduction reaction occurs at the working electrode (WE) due to the oxidants, while an oxidation reaction of the reductants simultaneously takes place at the counter electrode (CE). For the working electrode reaction, potassium ferricyanide ($K_3[Fe(CN)_6]$), containing ferricyanide ions as the oxidant, and potassium ferrocyanide trihydrate ($K_4[Fe(CN)_6]\cdot 3H_2O$), containing ferrocyanide ions as the reductant, were used. The oxidation-reduction reactions that occur when a voltage is applied to the working electrode in this electrolyte solution are as follows (Reiss and Hanratty, 1963):

$$Fe(CN)_6^{3-} + e \rightarrow Fe(CN)_6^{4-} \quad (1)$$

$$Fe(CN)_6^{3-} + e \rightarrow Fe(CN)_6^{4-} \quad (2)$$

The mass transfer coefficient is calculated from the current value obtained in this manner. To accurately derive the mass transfer coefficient, the three-electrode method was adopted, which allows for the precise measurement of current under a stable potential maintained by the reference electrode (RE). Furthermore, after confirming the plateau region using cyclic voltammetry (CV), the mass transfer coefficient is quantitatively determined from the limiting current, which is rate-limited by ion diffusion and measured within this region (Wang and Tsuji, 2024). In electrode reactions, ions are transported from the solution to the electrode surface mainly through migration due to the electric field, diffusion driven by the concentration gradient, and convection induced by the fluid flow. In the electrode reaction, the transport due to electrophoresis can be considered negligible compared to the transport due to the concentration gradient because the concentration of the supporting electrolyte is sufficiently high relative to the ion concentration. In addition, the flow in the y-direction, which is perpendicular to the wall, is very small compared to the mainstream flow. Therefore, by neglecting the effects of transport due to electrophoresis and convection due to y-direction flow, the ion mass transfer rate is expressed by the limiting current i as follows:

$$\tilde{k} = \frac{i}{An_eFc_b} \quad (2)$$

In the Eq. (3), A is the electrode area [m^2], n_e is the valence charge, F is the Faraday constant [C·mol^{-1}], c_b is the bulk ion concentration [mol·cm^{-3}].

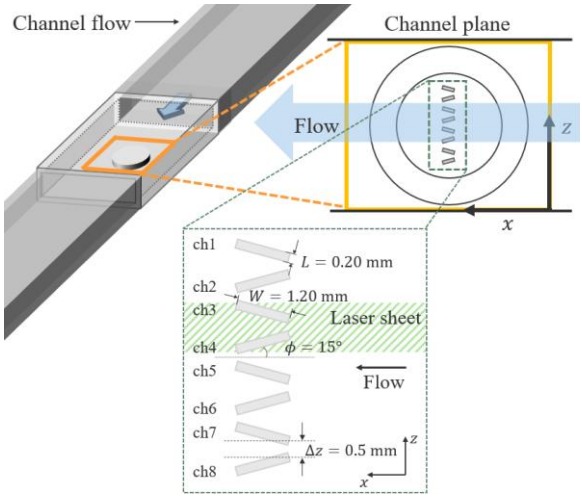

Figure 2. Schematic of the electrode configuration for the electrochemical method and the simultaneous measurement setup with PIV.

Determining the wall shear stress vector. The concentration boundary layer forms as a sufficiently thin layer only on the electrode surface, meaning its length is equal to the electrode length. For a sufficiently small point electrode, the concentration boundary layer thickness is minimal and resides within the viscous sublayer of the velocity boundary layer (Campbell and Hanratty, 1996). In this regime, the relationship between the velocity gradient and the mass transfer coefficient is given by Eq. (4), and the wall shear stress can be calculated from the velocity gradient using Eq. (5).

$$\tilde{k}_i = C\left(\frac{{D_f}^2\tilde{s}_i}{L_e}\right)^{\frac{1}{3}} \quad (3)$$

$$\tilde{\tau}_{w,i} = \frac{L_e\mu}{{D_f}^2}\left(\frac{\tilde{k}_i}{C}\right)^3 \quad (4)$$

where $i = x, z$, L_e represents the length of the concentration boundary layer. For a point electrode, L_e is equal to the equivalent length. D_f is the diffusion coefficient, C is a constant, $\tilde{s}$ is the velocity gradient ($\tilde{s} = \partial\tilde{u}/\partial y$), and the wall shear stress is calculated as $\tilde{\tau}_w = \mu\tilde{s}$. The constant C in Eqs. (4) and (5) accounts for the effects of electrode shape and size; for a point electrode, $C = 0.807$ (Wang and Tsuji, 2024; Reiss and Hanratty, 1963).

In this study, experiments were conducted to calculate both the streamwise and spanwise components of wall shear stress by slightly inclining rectangular electrodes from the flow direction and installing a pair of two rectangular electrodes in a V-shape (Campbell and Hanratty, 1996). Figure 2 shows a schematic of the electrodes. The working electrode plate is made of acrylic, and the rectangular electrodes have a width of 1.2 mm, a length of 0.2 mm, and were set at an angle of $\phi = 15°$ to the flow direction. Measurements were performed using these eight electrodes. The laser sheet was positioned as shown in Figure 2, and for the simultaneous measurements, the wall shear stress calculated from the electrode pair ch3 and ch4 through which the laser sheet passed was used.

Simultaneous Measurement

To measure the velocity field and wall shear stress simultaneously, the PIV and electrochemical measurement systems were set to the same sampling frequency. A trigger switch was used to enable simultaneous measurement. For simultaneous measurements, the analysis was performed exclusively at $Re_\tau = 180$, because the visualized particle images were accurately acquired.

Polymer concentrations and measurements conditions

Polyacrylamide was used as an additive to reduce the drag. Polyacrylamide is a type of flexible polymer known as an excellent drag-reducing agent, capable of achieving up to an 80% drag reduction effect. It does not ionize when added to water, making it possible to apply electrochemical measurement methods to the fluid. The polyacrylamide used in this study was from polymer additive, with a viscosity average molecular weight (MV) of 6×10^6. Polymers like polyacrylamide and other high-molecular-weight chains are susceptible to mechanical degradation, which can break the chains, reduce the average molecular weight, and thus decrease the drag reduction effect. To prepare the polymer solution, solid polyacrylamide particles were first dissolved in water under the stirring conditions specified in Table 1 to create a 3000 ppm stock solution. After letting it stand for a certain period, this polymer solution was added to the flow loop to prepare electrolyte solutions of different concentrations. The polymer concentration was varied in the actual experiments by adding different volumes of the stock solution. Table 1 shows the experimental parameters. Re_τ is the friction Reynolds number, defined as $Re_\tau = u_\tau h/\nu$. Here, h is the channel half-height, ν is the kinematic viscosity, ρ is the density, U_b is the bulk velocity, and u_τ is the friction velocity.

Table 1. Parameters for the experiments

U_b	(m/s)	0.54, 0.85, 1.19, 1.54
Re_τ	(-)	180, 260, 350, 440
Temperature	(℃)	20
Polymer concentration	(ppm)	0, 50, 100, 150, 200, 250, 300
Measurement time	(s)	60
Measurement Frequency	(Hz)	4000
Polymer (Polyacrylamide)		$M_v = 6\times10^6$

RESULTS

Drag reduction observations

The instantaneous wall shear stress obtained from seven measurement points were averaged to calculate the mean wall shear stress $\overline{|\tilde{\boldsymbol{\tau}}_{\boldsymbol{w}}|}$. Subsequently, the friction coefficient C_f was evaluated for each concentration, and the drag reduction rate (DR) was determined. The definitions are as follows:

$$C_f = \frac{\overline{|\tilde{\boldsymbol{\tau}}_{\boldsymbol{w}}|}}{1/2\,\rho {U_b}^2} \tag{6}$$

$$DR = \frac{C_{f,0\text{ppm}} - C_{f,\text{polymer}}}{C_{f,0\text{ppm}}} \times 100\%. \tag{7}$$

The results showed that the drag reduction rate increased with both Reynolds number and polymer concentration. At a friction Reynolds number of $Re_\tau = 180$ and a polymer concentration of 300 ppm, the drag reduction rate was approximately 10%. The maximum drag reduction observed was about 21% at $Re_\tau = 440$ with a polymer concentration of 300 ppm.

Mean velocity profile

The instantaneous stream-wise velocity was averaged at different wall-normal locations to create the mean velocity profile, as shown in Figure 3. It was found that as the polymer concentration increased, the velocity in the near center region increased, and the mean velocity profiles became steeper in the near-wall region. As a result, it was concluded that the thickness of the buffer layer increased with increasing polymer concentration.

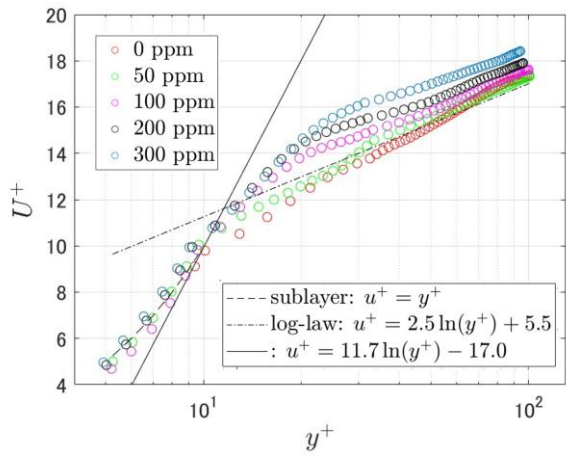

Figure 3. Comparison of mean velocity profiles at $Re_\tau = 180$ for different polymer concentrations.

Pre-multiplied energy spectrum

Spectral analysis was conducted to evaluate the energy distribution in turbulent flow and the influence of polymer additives on different scales. In this study, the power spectral density $P(f)$ was calculated from the time-series data of wall shear stress, and the pre-multiplied spectrum (PMS), defined as $fP(f)$, was used to evaluate the energy distribution. The PMS represents the contribution of each frequency band to the total energy on a logarithmic frequency scale and is useful for identifying dominant scales.

The PMS was calculated in both the streamwise and spanwise directions from the time-series data of wall shear stress. The results at $Re_\tau = 440$ are shown in Figure 4. Figure 4(a) shows the PMS of the streamwise wall shear stress, while Figure 4(b) shows that of the spanwise wall shear stress. As the polymer concentration increases, the peak value of the PMS decreases. This result indicates that the energy of the near-wall flow is weakened by the addition of polymers. And the peak position slightly shifts toward the lower-frequency side with increasing polymer concentration. This shift suggests that the dominant scale in the near-wall region changes from small scales corresponding to high frequencies to larger scales corresponding to lower frequencies. Therefore, it is inferred that the addition of polymers suppresses the generation of small-scale vortices and the progression of the energy cascade, resulting in larger-scale structures becoming dominant.

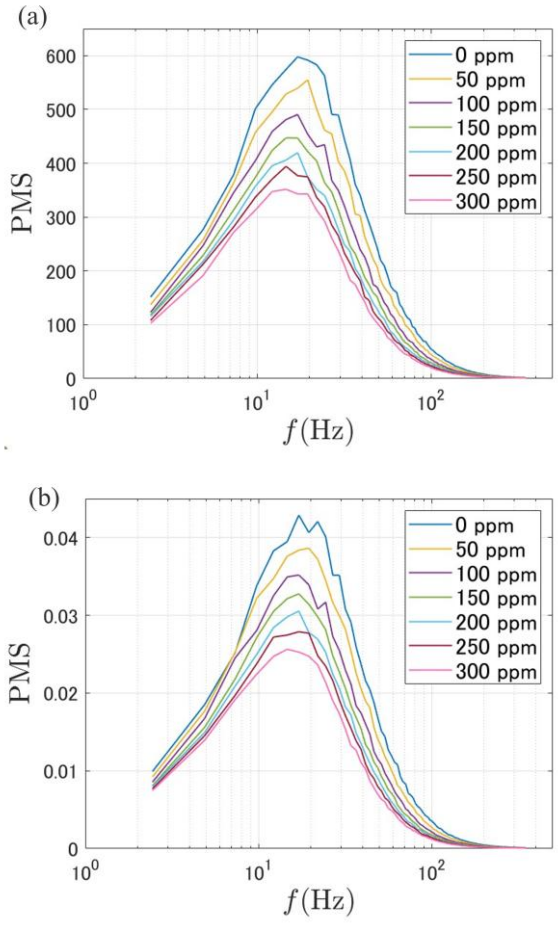

Figure 4. Pre-multiplied spectra of wall shear stress fluctuation $Re_\tau = 440$. (a) Streamwise component. (b) Spanwise component.

Simultaneous Measurement

Cross-correlation coefficient. To investigate the correlation between the velocity field and the wall shear stress in the streamwise direction, the cross-correlation coefficient was calculated. The equation for calculating the cross-correlation coefficient is defined by Eq. (8).

$$R_{u\tau_{w,x}}(\Delta t) = \frac{\overline{\tau_{w,x}'(t)\, u'(t+\Delta t)}}{\sqrt{\overline{\tau_{w,x}'^2}}\sqrt{\overline{u'^2}}} \tag{8}$$

where the streamwise wall shear stress, $\tau_{w,x}'(t)$, measured at time t, and the streamwise velocity component, $u'(t+\Delta t)$, which passed directly over the measurement point Δt seconds earlier. By calculating the cross-correlation coefficient for each height from the wall, we can also use an iso-surface to confirm how a velocity u' at an arbitrary distance from the wall influences the wall shear stress $\tau_{w,x}'$ with a minute time delay.

Cross correlation coefficient is plotted in Figure 5 where the horizontal axis indicates the stream-wise distance based on Taylor's frozen hypothesis. At a polymer concentration of 0 ppm, a region of high correlation was observed extending beyond the near-wall region into the buffer layer. In contrast, at 150 ppm, the correlation between the velocity field and the wall shear stress decreased markedly in the near-wall region. At 300 ppm, the fluctuations in wall shear stress showed little correlation with the near-wall velocity. These results indicate that the influence of the velocity field on the wall shear stress is weakened by polymer additives. This interpretation is consistent with other observed phenomena, such as the thickening of the buffer layer and the suppression of large wall shear stress fluctuations with increasing polymer concentration. A similar correlation analysis was also conducted between the spanwise wall shear stress and velocity fluctuations; however, no clear effect of polymer addition was identified. This may be attributed to the difficulty in accurately measuring the wall-normal velocity component. Therefore, further measurements in the near-wall region are planned in future work.

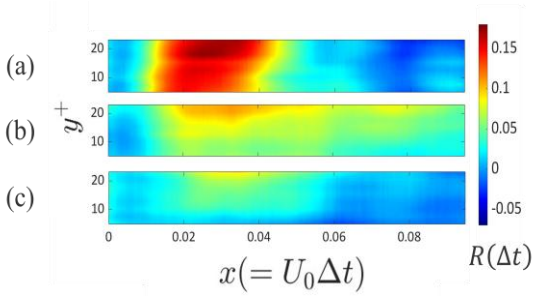

Figure. 5 Contour plots of the cross-correlation between velocity and wall shear stress. (a) 0 ppm, (b) 150 ppm, (c) 300 ppm.

CONCLUSION

In this study, the velocity field and wall shear stress were measured at several polymer concentrations using Particle Image Velocimetry (PIV) and an electrochemical measurement technique. Simultaneous measurements with these two methods were conducted to investigate the correlation between the velocity field and wall shear stress.

Polyacrylamide was used as the polymer additive, resulting in a maximum drag reduction of approximately 21%. As the polymer concentration increased, large fluctuations in wall shear stress were suppressed in both the streamwise and spanwise directions. Furthermore, the mean velocity profiles indicated an increase in the thickness of the buffer layer.

In addition, the correlation between the velocity and wall shear stress fluctuations was analyzed using the cross-correlation coefficient. The results showed that, particularly in the near-wall region, the correlation between the velocity field and wall shear stress decreased as the polymer concentration increased. These findings suggest that polymers play a role in inhibiting the transmission of flow-field influences to the wall in the near-wall region.

ACKNOLEDGEMENT

This work was supported in part by JSPS KAKENHI Grant Numbers JP23K26323.

REFERENCES

Hutchins, N. and Marusic, I., 2007, "Evidence of very long meandering features in the logarithmic region of turbulent boundary layers", *Journal of Fluid Mechanics,* Vol. 579, pp. 1-28.

Toms, B., 1949, "Some Observations on the Flow of Linear Polymer Solutions Through Straight Tubes at Large Reynolds Numbers," *Nature*, Vol. 2, pp. 135–141.

Kline, S. J., Reynolds, W. C., Schraub, F. A., and Runstadler, P. W., 1967, "The Structure of Turbulent Boundary Layers," *Journal of Fluid Mechanics*, Vol. 30, pp. 741–773.

Li, X., 2019, "Turbulent Drag Reduction by Polymer Additives: Fundamentals and Recent Advances," *Physics of Fluids*, Vol. 31, 121302.

Kim, K., Islam, M. T., Shen, X., Sirviente, A. I., and Solomon, M. J., 2004, "Effect of Macromolecular Polymer Structures on Drag Reduction in a Turbulent Channel Flow," *Physics of Fluids*, Vol. 16, pp. 4150–4162.

Kim, K., and Sirviente, A. I., 2005, "Turbulence Structure of Polymer Turbulent Channel Flow With and Without Macromolecular Polymer Structures," *Experiments in Fluids*, Vol. 38, pp. 739–749.

Mathis, R., Hutchins, N., and Marusic, I., 2009, "Large-Scale Amplitude Modulation of the Small-Scale Structures in Turbulent Boundary Layers," *Journal of Fluid Mechanics*, Vol. 628, pp. 311–337.

Wang, Y., and Tsuji, Y., 2024, "Characteristics of Shear Stress Fluctuations in Polymer Solutions and Their Relation to Turbulent Structures in Channel Flows," *Physics of Fluids*, Vol. 36, 105153.

Reiss, L. P., and Hanratty, T. J., 1963, "An Experimental Study of the Unsteady Nature of the Viscous Sublayer," *AIChE Journal*, Vol. 9, p. 154.

Campbell, J. A., and Hanratty, T. J., 1996, "Measurement of Wall Shear Stress," in *Fluid Mechanics Measurements*, 2nd ed., Routledge.